Electronic Supplementary Information

Enhanced proton conductivity in a flexible metal-organic framework promoted by single-crystal-to-single-crystal transformation

Xi Chen,[a] Zhongyue Zhang,[b]* Jin Chen,[a] Sergei Sapchenko,[a] Xue Han,[a] Ivan da-Silva,[c] Ming Li,[d] Inigo J. Vitorica-Yrezabal,[a] George Whitehead,[a] Chiu C. Tang,[e] Kunio Awaga,[b] Sihai Yang,[a]* and Martin Schröder[a]*

a Department of Chemistry, University of Manchester, Manchester, M13 9PL, U.K. Sihai.Yang@manchester.ac.uk; M.Schroder@manchester.ac.uk

b Department of Chemistry, Nagoya University, Furocho, Chikusa, 464-8602, Nagoya, Japan. zhang.zhongyue@i.mbox.nagoya-u.ac.jp

c ISIS Pulsed Neutron and Muon Source, Rutherford Appleton Laboratory, Oxfordshire OX11 0QX, U.K.

d School of Engineering, University of Nottingham, Nottingham NG7 2RD, U.K.

e Diamond Light Source, Harwell Science Campus, Oxfordshire, OX11 0DE, U.K.

Materials and Characterisations

Starting materials were purchased from Acros Organics and Sigma-Aldrich and used without further purification. The ligand was synthesised based on our pervious report.[1] ATR-IR spectra were collected on a Thermo Scientific Nicolet iS5-IR spectrometer in the range from 4000 cm^{-1} to 400 cm^{-1}, and TGA plots were collected on a Perkin Elmer Pyris1 thermogravimetric analyser under N_2 at a flow rate of 100 mL/min and heating rate of 5 °C /min. Elemental analyses were performed on a Flash 2000 elemental analyser, and BET surface areas were obtained from N_2 adsorption/desorption isotherms recorded on a Micromeritics 3-Flex instrument at 77 K. Water adsorption/desorption isotherms were performed on Micromeritics 3Flex Surface Area Analyser at 298 K.

Single crystal X-ray data were collected at 150 K on a GV1000 Oxford-Rigaku Supernova diffractometer with Mo-Kα (λ = 0.71073Å) and at 100 K using Rigaku FR-X diffractometer with Cu-Kα (λ = 1.5418Å) equipped with a CCD detector and an Oxford Cryosystems liquid N_2 flow system. Data collection, frame integration and data processing were performed using CrysAlisPro program suite.[2] The structure was solved by direct method and refined on F^2 by full-matrix least-squares method in the anisotropic approximation (for non-hydrogen atoms) using Olex2 program package.[3] The positions of hydrogen atoms of organic ligands were calculated geometrically and refined by a riding model. A summary of the crystallographic data and structural determination for all the compounds is provided in Table S1.

X-ray powder diffraction patterns were collected on a Phillips X'pert Pro MPD powder diffractometer using a plate sample holder at room temperature. High-resolution synchrotron X-ray powder diffraction (SXPD) data of were collected on Beamline I11 Diamond Light Source at room temperature.

Proton conductivity measurements were performed on a Solartron SI1260 Impedance analyser over a frequency range of 1 Hz to 1 MHz at the amplitude of 100 mV under the DC rest voltage of 0 mV. The Impedance analyser was connected by an electrochemical cell equipped with platinum current collectors, and the temperature and relative humidity inside the cell was measured using a Rotronic HC2-C04 probe. The pellets were prepared by a press machine under 3 tons to give a thickness of ~1 mm and diameter of 8 mm. The top surface and bottom surface were both coated silver paste.

AC impedance analyses of single crystals were performed on a Biologic SP-150 potentiostat with a low current option over a frequency range of 0.1 Hz to 200 kHz at an amplitude of 200 mV and 0 mV DC rest voltage.

Dielectric constant measurements were also performed on a Solartron SI1260 Impedance analyser by using the same rig as the proton conductivity measurement under N_2 with a flow rate of 50 mL/min (0 %RH). The dielectric constant (ε) is calculated from the electrical capacitance (C) according to equation (1).

$$C = \varepsilon_r \cdot \varepsilon_0 \cdot \frac{A}{d} \quad (1)$$

where *C* is capacitance, ε_r is the relative dielectric constant (the real dielectric constant of the sample), ε_0 is dielectric constant of vacuum (ε_0= 8.85×10^{-12} F/m), A is the cross-sectional area of the sample pellet, and *d* is the thickness of the pellet.

Synthesis of MFM-722(Pb)-DMA [$Pb_2(L)(DMA)_2$]

H_4L (biphenyl-3,3',5,5' tetracarboxylic acid) (0.033 g, 0.10 mmol) and $Pb(NO_3)_2$ (0.066 g, 0.20 mmol) were dissolved in a mixture of DMA (2 mL, N,N-dimethylacetamide), NMP (1 mL, 1-Methyl-2-pyrrolidinone) and dilute nitric acid (0.5 mL, 5%). The mixture was transferred into a pressure vial (8 mL) and heated at 90 °C for 3 days, then cooled down to room temperature. The colourless single crystals were collected by filtration and dried in air. Yield: 0.073 g (0.08 mmol), 80 %. Elemental analysis and ICP (%): Anal. Calc. for $C_{20}H_{25}O_{10}N_2Pb_2$: C 26.23, H 2.73, N 3.06, Pb 45.30; Found: C 26.70, H 2.56, N 3.14, Pb 44.92. ATR-IR for MFM-722(Pb)-DMA (Fig. S14): 3081(w), 2927(w), 2876(w), 1644(m), 1592(m), 1343(s), 1073(m), 1017(m), 908(w), 811(m), 773(s), 711(s).

Preparation of MFM-722(Pb)-H$_2$O [$Pb_2(L)(H_2O)$]

The single crystals of MFM-722(Pb)-H_2O were obtained by soaking single crystals of MFM-722(Pb)-DMA in water for 3 h or exposing to water vapour for 10 h at 25 °C. The bulk samples of MFM-722(Pb)-H_2O can be synthesized by soaking powder of MFM-722(Pb) in water for 1.5 days at 150 °C. Elemental analysis and ICP (%): Anal. Calc. for $C_{16}H_8O_9Pb_2$: C 25.31, H 1.05, N 0.00, Pb 54.63; Found: C 26.70, H 1.20, N 0.05, Pb 53.09. ATR-IR for MFM-722(Pb)-H_2O (Fig. S14): 3610(w), 3431(w), 3040(w), 1609(m), 1598(m), 1354(s), 1085(m), 930(m), 901(m), 831(s), 772(s), 721(s).

Preparation of MFM-722(Pb) [$Pb_2(L)$]

MFM-722(Pb) can be obtained by heating MFM-722(Pb)-DMA at 150 °C for 12 h under vacuum. The single crystals decayed during the activation, so the crystal structure was determined by high-resolution synchrotron X-ray powder diffraction (SXPD) data. Elemental analysis and ICP (%): Anal. Calc. for $C_{16}H_6O_8Pb_2$: C 25.92, H 0.81, N 0.00, Pb 55.95; Found: C 26.70, H 1.00, N 0.02, Pb 56.20.

Crystallographic data

Table S1. Summary of crystallographic data

Name	MFM-722(Pb)-DMA	MFM-722(Pb)-H_2O	MFM-722(Pb)
Formula	$C_{24}H_{24}N_2O_{10}Pb_2$ $[Pb_2(L)(DMA)_2]$	$C_{16}H_8O_9Pb_2$ $[Pb_2(L)(H_2O)]$	$C_{16}H_6O_8Pb_2$ $[Pb_2(L)]$
Radiation	MoKα ($\lambda = 0.7107$)	CuKα ($\lambda = 1.5418$)	Synchrotron ($\lambda = 0.824869$)
M, g/mol	914.85	758.62	740.60
Crystal system	Triclinic	Triclinic	Monoclinic
Space group	$P\bar{1}$	$P\bar{1}$	$C2/m$
a, Å	10.4855(4)	7.3121(17)	9.3908(7)
b, Å	11.1137(5)	9.4816(17)	18.8473(8)
c, Å	12.4920(4)	11.803(3)	4.6739(3)
α, deg	111.886(4)	81.482(17)	90
β, deg	101.798(3)	74.95(2)	118.995(5)
γ, deg	103.943(4)	73.334(18)	90
V, $Å^3$	1239.04(11)	754.6(3)	723.55(8)
Z	2	2	2
D(calcd), g/cm^3	2.452	3.338	3.399
μ, mm^{-1}	13.632	43.406	
F(000)	852.0	680.0	
Crystal size, mm^3	0.248 × 0.123 × 0.051	0.240 × 0.051 × 0.031	Powder
Temperature, K	150 K	100 K	298 K
Index ranges	$-13 \leq h \leq 13$, $-13 \leq k \leq 13$, $-15 \leq l \leq 15$	$-9 \leq h \leq 9$, $-11 \leq k \leq 11$, $-14 \leq l \leq 14$	
Reflections collected	24359	5354	
Independent reflections	7619	5354	
Goodness-of-fit on F^2	1.018	1.182	1.557
Final R indexes [$I>=2\sigma(I)$]	$R_1 = 0.0358$, $wR_2 = 0.0918$	$R_1 = 0.1003$, $wR_2 = 0.2797$	$R_p = 0.0133$; $R_{wp} = 0.0179$; $R_{exp} = 0.0115$
CCDC	1995412	1995413	2018703

Co-ordination environment of ligands

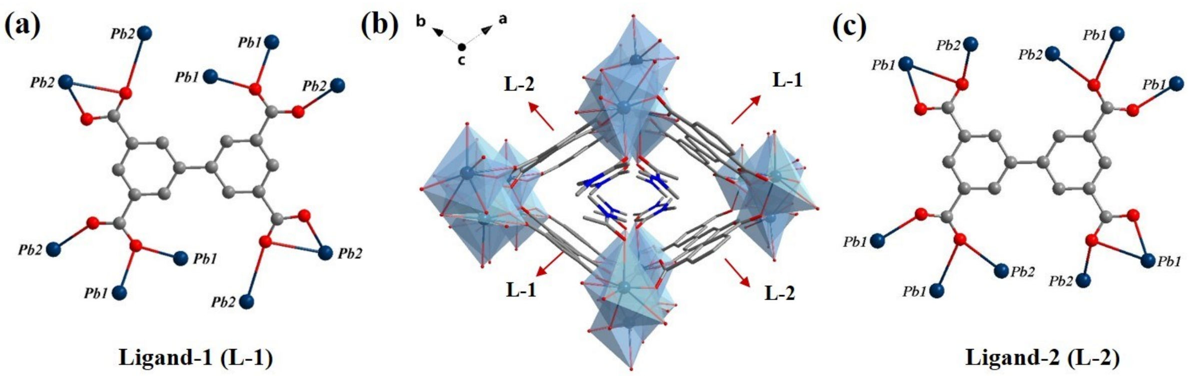

Fig. S1. View of two crystallographically-independent ligands in MFM-722(Pb)-DMA. (a) Co-ordination environment of Ligand-1 (L-1); (b) view of the structure of MFM-722(Pb)-DMA along the *c*-axis; (c) co-ordination environment of Ligand-2 (L-2).

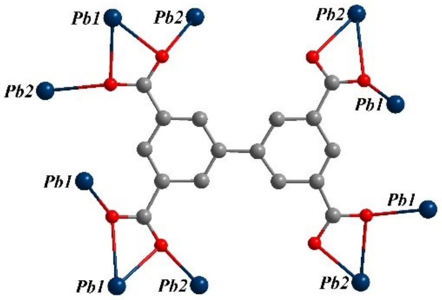

Fig. S2. Ligand co-ordination environment in MFM-722(Pb)-H_2O.

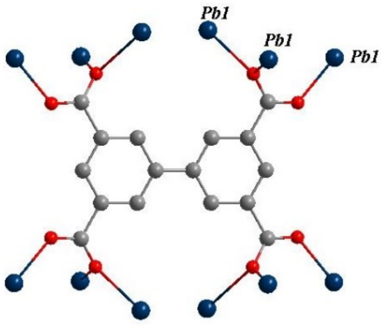

Fig. S3. Ligand co-ordination environment in MFM-722(Pb).

Co-ordination environment of Pb centres

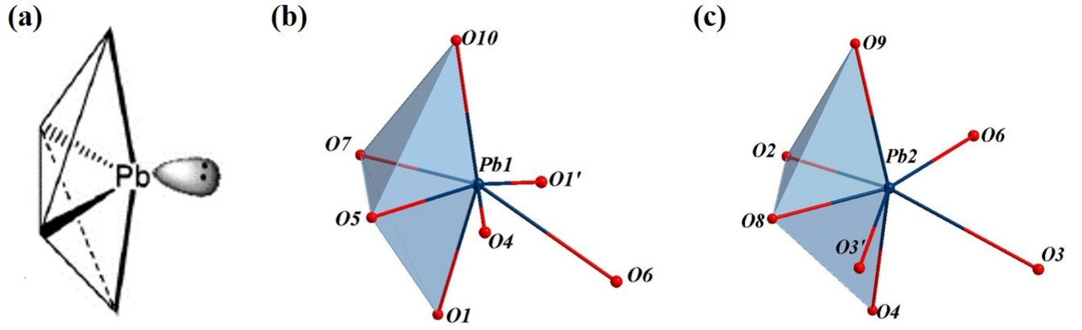

Fig. S4 Views of (a) ψ-trigonal bipyramid co-ordination polyhedra (ψ-TBP), and (b, c) co-ordination environment of Pb(1) and Pb(2) in MFM-722(Pb)-DMA.

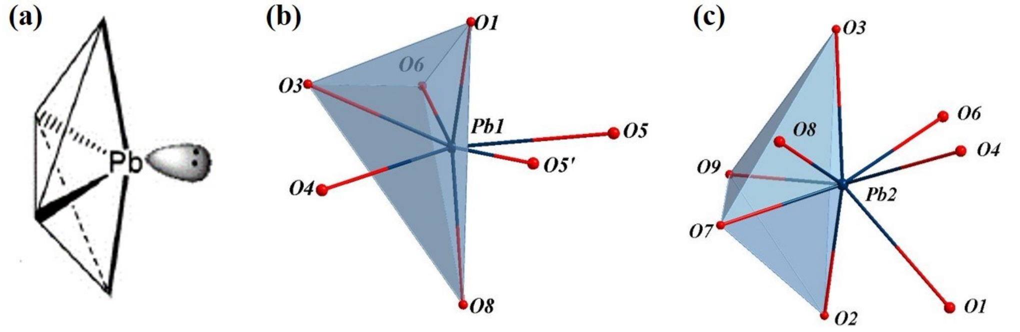

Fig. S5 Views of (a) ψ-trigonal bipyramid co-ordination polyhedra (ψ-TBP), and (b, c) co-ordination environment of Pb(1#) and Pb(2#) in MFM-722(Pb)-H_2O.

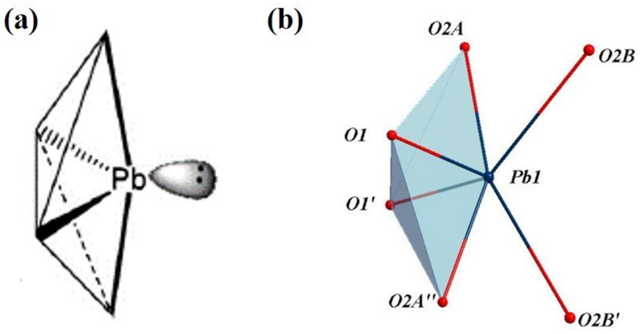

Fig. S6 Views of (a) ψ-trigonal bipyramid co-ordination polyhedra (ψ-TBP), and (b) co-ordination environment of Pb(1) in MFM-722(Pb).

Table S2 Summary of bond lengths and bond angles

Compounds		MFM-722(Pb)-DMA		MFM-722(Pb)-H_2O		MFM-722(Pb)
Pb atoms		Pb(1)	Pb(2)	Pb(1#)	Pb(2#)	Pb (1)
Overall co-ordination number		7 (4+E)+3	7 (4+E)+3	7 (4+E)+3	8 (4+E)+4	6 (4+E)+2
Shape of the polyhedron		ψ-TBP	ψ-TBP	ψ-TBP	ψ-TBP	ψ-TBP
Pb–O bond distances in the polyhedron (Å)	Axial	2.354 (6) O(1) 2.648 (7) O(10)	2.397 (6) O(4) 2.597 (8) O(9)	2.54 (2) O(1) 2.59 (2) O(8)	2.48 (2) O(2) 2.69 (3) O(3)	2.620 (12) O(2A) 2.620 (12) O(2A′)
	Equatorial	2.416 (6) O(5) 2.346 (6) O(7)	2.373 (6) O(2) 2.353 (6) O(8)	2.57 (2) O(3) 2.49 (2) O(6)	2.468 (19) O(7) 2.63 (3) O(9)	2.197 (9) O(1) 2.197 (9) O(1′)
Bond angles O–Pb–O (◦) in the polyhedron between the atoms	Axial	155.4 (3) O(1)-Pb(1)-O(10)	155.1 (2) O(4)-Pb(2)-O(9)	137.1 (7) O(1)-Pb(1)-O(8)	156.1 (9) O(2)-Pb(2)-O(3)	154.021 (337) O(2A)-Pb-O(2A′)
	Equatorial	79.4 (2) O(5)-Pb(1)-O(7)	74.04 (19) O(2)-Pb(2)-O(8)	73.3 (7) O(3)-Pb(1)-O(6)	70.2 (7) O(7)-Pb(2)-O(9)	79.653 (276) O(1)-Pb-O(1′)
Pb–O secondary bonds (Å)		2.754(6) O(1′) 2.903 (7) O(4) 2.776 (6) O(6)	2.925 (8) O(3) 2.904 (9) O(3′) 2.774 (6) O(6)	2.70 (3) O(4) 2.66 (2) O(5) 2.68 (2) O(5′)	2.889 (26) O(1) 2.73 (3) O(4) 2.742 (18) O(8) 2.77 (2) O(9)	2.845 (11) O(2B) 2.845 (11) O(2B′)

E, lone pair of electrons;
ψ-TBP, ψ-trigonal bipyramid, trigonal bipyramid with a vacant vertex in the equatorial plane.

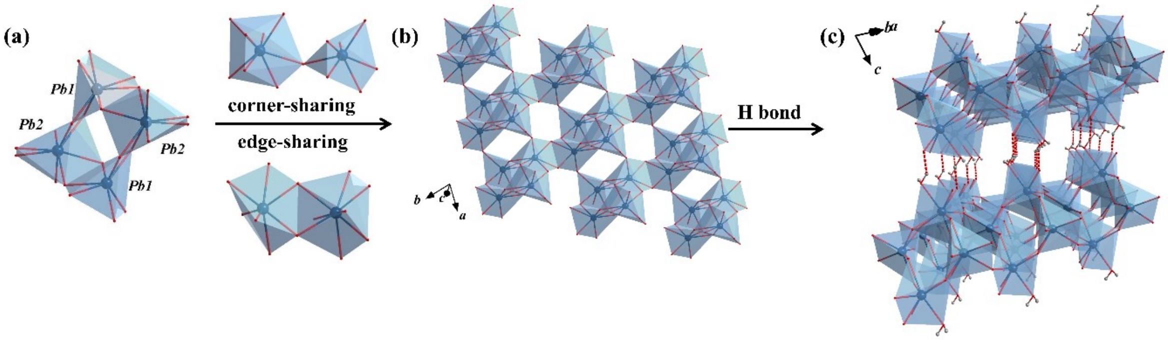

Fig. S7 View of 2D layers of $[Pb_4O_{18}]_\infty$ in MFM-722(Pb)-H_2O: (a) tetra-nuclear clusters; (b) lead oxide layer derived from tetra-nuclear clusters corner-sharing and edge-sharing along the *c* axis; (c) packing of layers of $[Pb_4O_{18}]_\infty$ through the H-bonds interactions (O9-H···O2) along the *ab* plane.

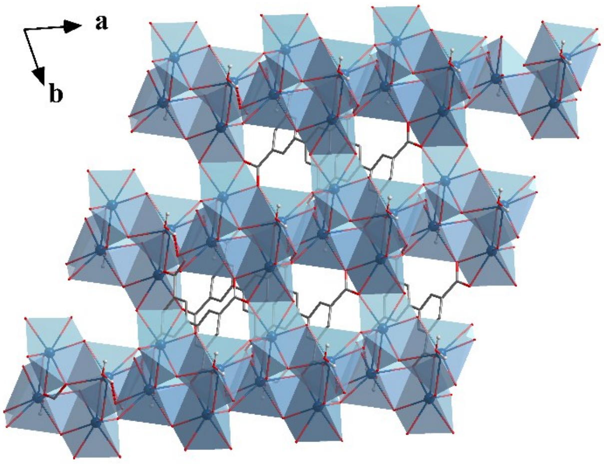

Fig. S8 View of the structure of MFM-722(Pb)-H_2O along the *c* axis

There is no proton transfer pathway along c axis. Thus, the proton conductivity along the *c* axis will be lower than that along the *a* axis.

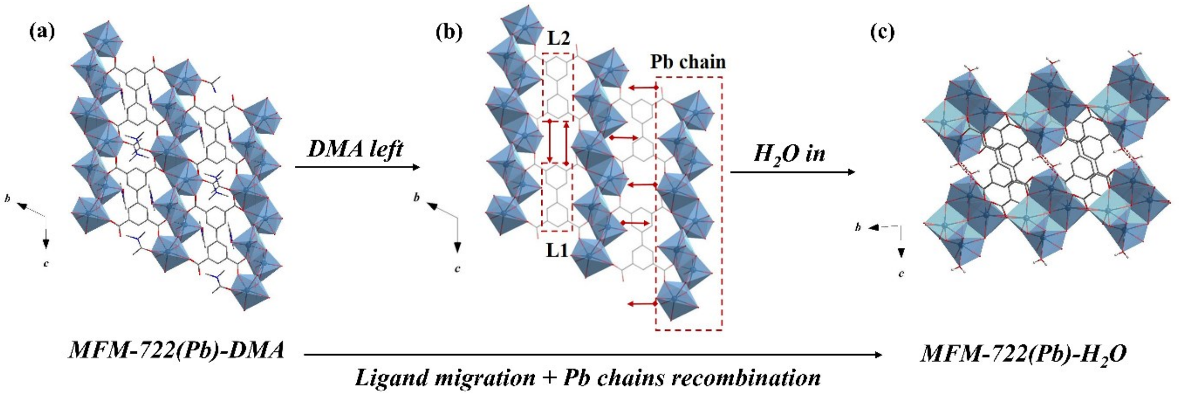

Fig. S9 Schematic illustration of potential mechanism of SCSC transformation: (a) structure of MFM-722(Pb)-DMA viewed along *a* axis; (b) potential ligand migration; (c) structure of MFM-722(Pb)-H_2O viewed along the *a* axis.

When MFM-722(Pb)-DMA is immersed in water, the co-ordinated DMA molecules are exchanged gradually by the H_2O molecules to generate MFM-722(Pb)-H_2O. Loss of DMA affords space between the adjacent ligands (L1 and L2) leading to a shift in L1 and L2 (Fig. S9b) and the two parallel Pb chains coming closer to each other to form layers of $[Pb_4O_{18}]_\infty$ in MFM-722(Pb)-H_2O (Fig. S9c).

Table S3 Summary of O···O bond distances in the supra-octahedron in MFM-722(Pb)-H_2O

O···O bonds	distances (Å)
O9···O2*	2.837 (34)
O9···O9*	3.504 (43)
O9···O2	3.047 (43)
O9···O7	2.923 (39)
O9···O7*	2.889 (29)

Table S4 Summary of hydrogen bonds in MFM-722(Pb)-H_2O

D	H	A	d(D−H)/Å	d(H−A)/Å	d(D−A)/Å	D−H−A/°
O9*	H9A*	O2	0.875 (26)	2.085 (24)	2.837 (34)	143.8 (17)
O9	H9A	O2*				
O9	H9A	O9*	0.875 (26)	2.787 (31)	3.504 (43)	140.2 (19)
O9*	H9A*	O9				

The position of H atom is refined geometrically and subject to rotation.

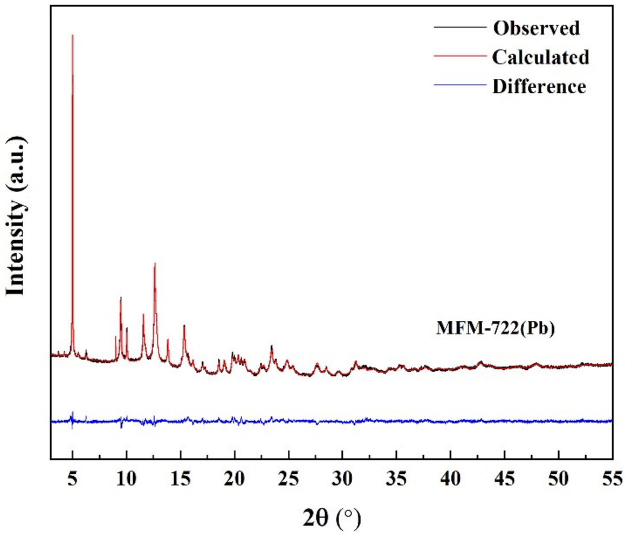

Fig. S10 Synchrotron PXRD patterns [observed (grey), calculated (red) and difference (blue)] for Rietveld refinement of the model of MFM-722(Pb) [λ = 0.824869 (2) Å].

N_2 adsorption/desorption isotherms of MFM-722 (Pb)-H_2O

Prior to the BET measurement, the bulk MFM-722(Pb)-H_2O was activated under vacuum at 120 °C for 12 h. The adsorption-desorption isotherms for N_2 was carried out at 77 K. Fig. S11 shows a type-III profile with a surface area of ~32 m^2 g^{-1}.

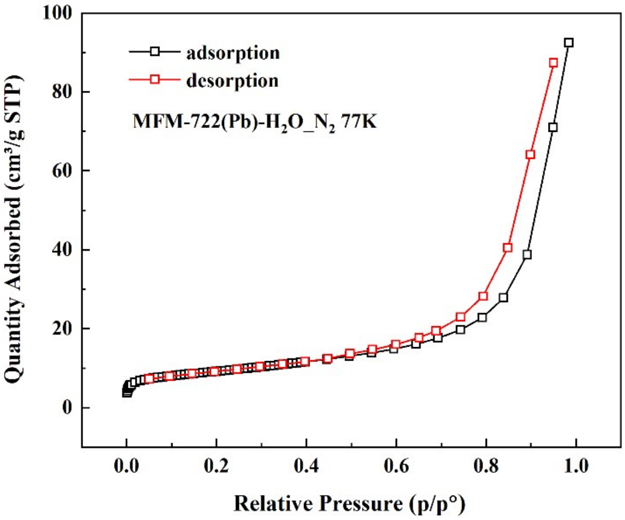

Fig. S11 Adsorption and desorption isotherms for N_2 in MFM-722(Pb)-H_2O at 77 K

Water adsorption/desorption isotherms of MFM-722 (Pb)-H_2O

MFM-722(Pb)-H_2O was washed with acetone at 25 °C to remove surface water and then activated under vacuum at 80 °C for 12 h. Fig. S12a shows a type-II profile with a total water uptake of 3.32 mmol g^{-1} at 298 K. Fig. S12b shows that MFM-722(Pb)-H_2O shows a full retention of its crystal structure after the activation.

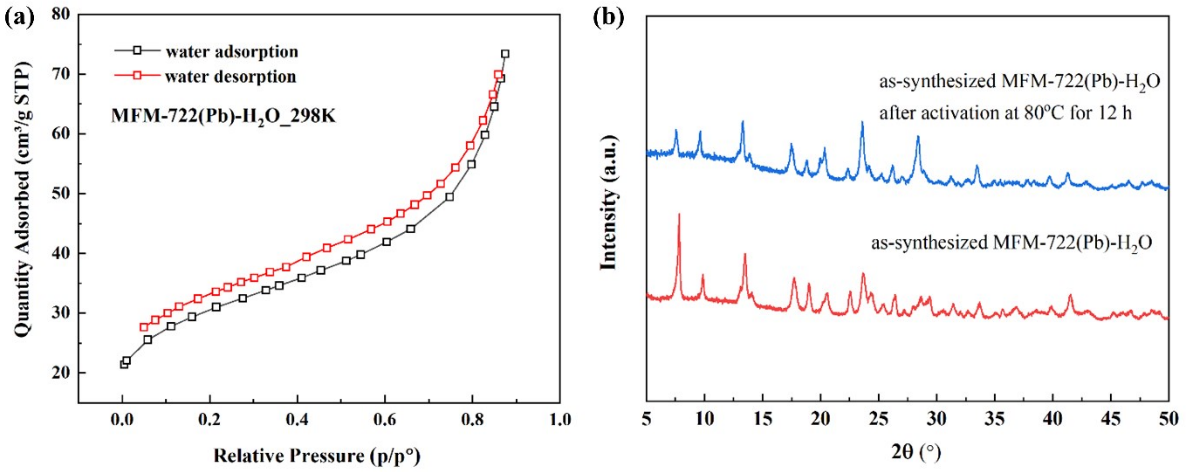

Fig. S12 (a) Adsorption and desorption isotherms for water in MFM-722(Pb)-H_2O at 298 K; (b) PXRD patterns for MFM-722(Pb)-H_2O and after activation at 80 °C for 12 h.

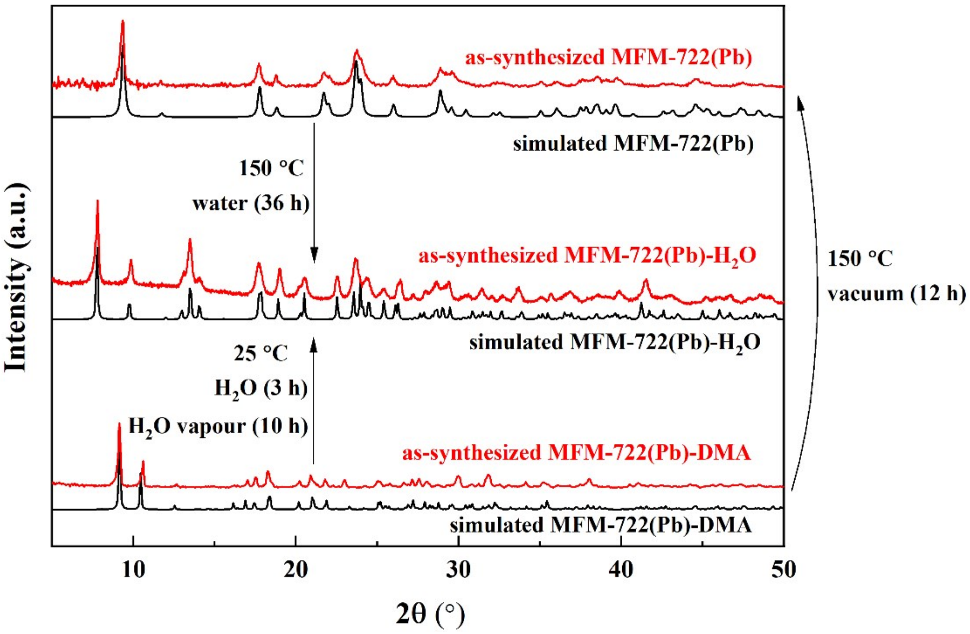

Fig. S13 PXRD patterns of as-synthesized MOFs (red) and simulations (black). The PXRD patterns recorded at 298 K (as-synthesized) match the simulated data based upon the single crystal structure obtained at 100 K for the MFM-722(Pb)-H_2O.

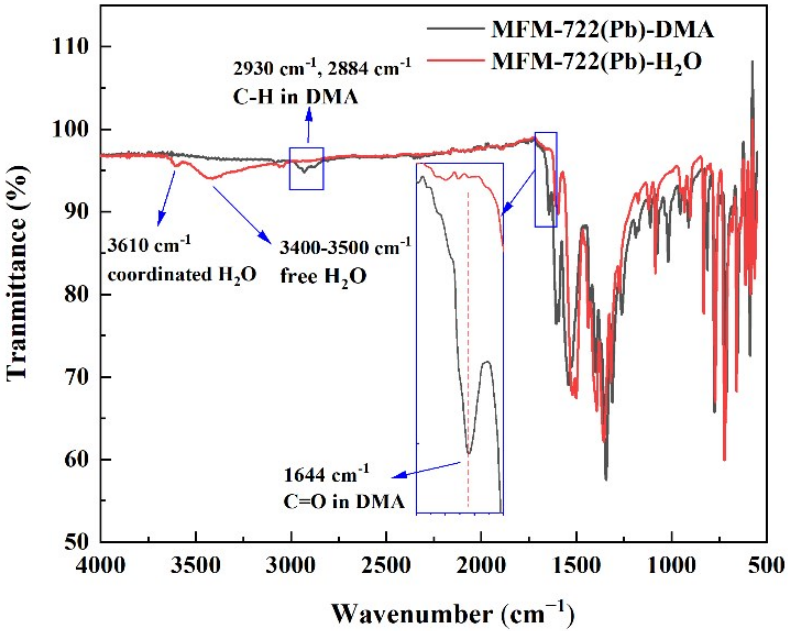

Fig. S14 ATR-IR spectra of MFM-722(Pb)-DMA (black) and MFM-722(Pb)-H_2O (red).

Vibrations due to the OH moieties of co-ordinated water in MFM-722(Pb)-H_2O appear at 3610 cm^{-1}. The broad band centred at 3431 cm^{-1} is assigned to the stretching vibration of -OH moieties of free water molecules in MFM-722(Pb)-H_2O. The peaks assigned to the ν(C-H) stretch of methyl groups are observed at 2930 cm^{-1} and 2844 cm^{-1} in MFM-722(Pb)-DMA. The peak at 1644 cm^{-1} is assigned to the ν(C=O) stretching vibration in DMA, which is not present in MFM-722(Pb)-H_2O.

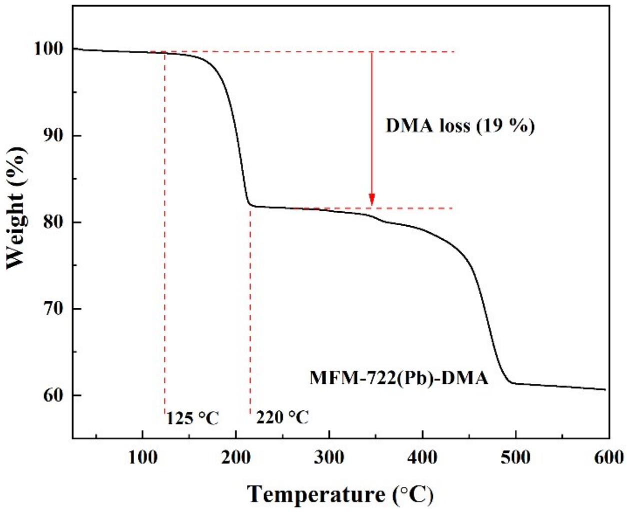

Fig. S15 TGA plot of MFM-722(Pb)-DMA

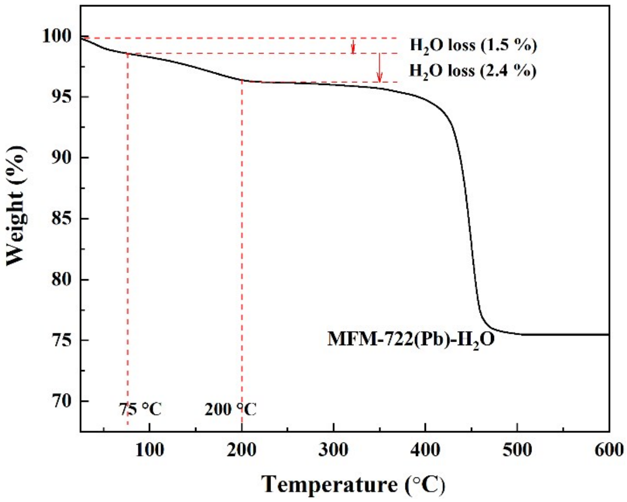

Fig. S16 TGA plot of MFM-722(Pb)-H_2O

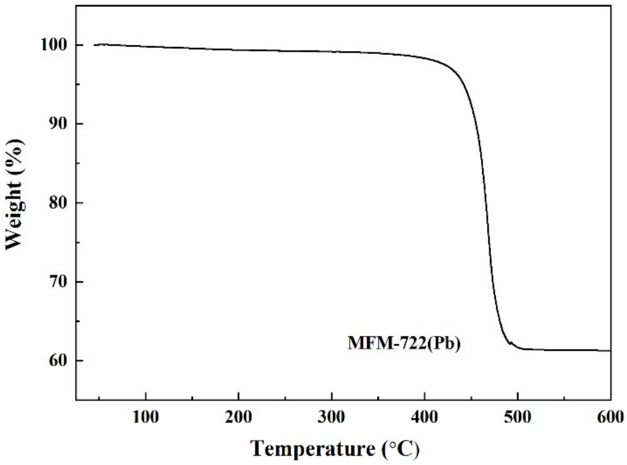

Fig. S17 TGA plot of MFM-722(Pb)

Proton conductivity measurement of single crystals of MFM-722(Pb)-DMA

AC impedance spectroscopy was employed to assess the change in proton conductivity of MFM-722(Pb)-DMA *in situ* during the SCSC transformation. Measurements were carried out on two single crystals of MFM-722(Pb)-DMA by using the conventional two-probe method[4] (Fig. S18a). The dimensions of the single crystal of MFM-722(Pb)-DMA in Fig. 2a was estimated to be 468 × 64 × 54 μm^3. The dimensions of the single crystal of MFM-722(Pb)-DMA in Fig. 2b-d was estimated to be 325 × 41 × 31 μm^3. Face indexing results of MFM-722(Pb)-DMA and MFM-722(Pb)-H_2O are shown in Fig. S18b and S18c, respectively. After SCSC transformation, the crystallographic *c* axis is still along the long dimension of the crystal, which is the direction of the proton conductivity measurement.

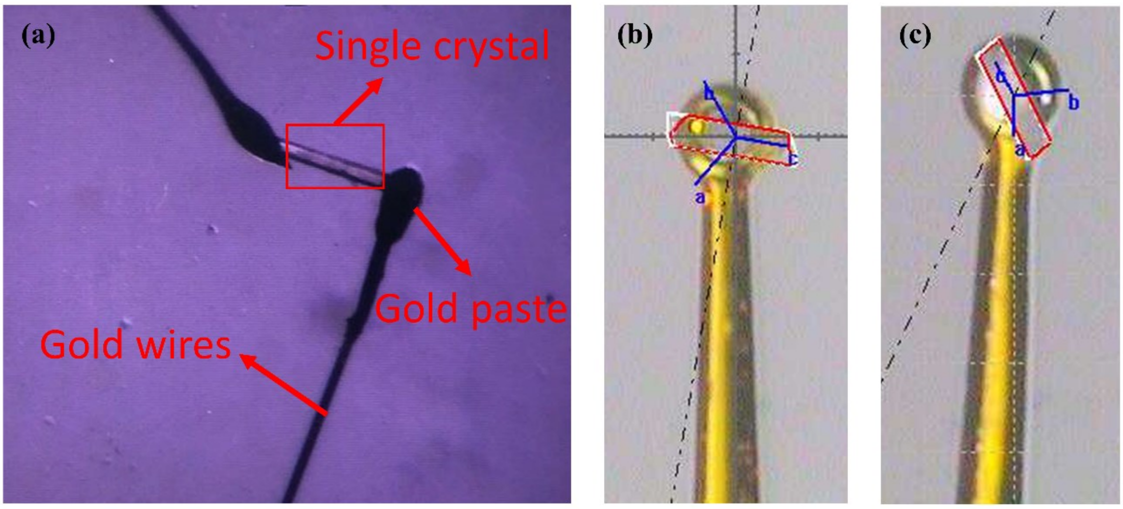

Fig. S18 (a) Fabrication of the single crystal of MFM-722(Pb)-DMA using the two-probe method. (b and c) Analysis of the face indices of single crystals of MFM-722(Pb)-DMA and MFM-722(Pb)-H_2O, respectively.

The proton conductivity (σ) can be calculated *via* the electrical resistance (R) according to equation (2). L is the length between the two electrodes and A is the cross-sectional area.

$$\sigma = \frac{1}{R} \times \frac{L}{A} \tag{2}$$

For the single crystal in Fig. 2a ($468 \times 64 \times 54$ μm^3), the cross-sectional area (A) is 3.456×10^{-5} cm^2, the length (L) is 4.68×10^{-2} cm; the resistance (R) and proton conductivity (σ) results are summarised in Table S5.

Table S5 Summary of proton conductivity measurements of single crystals during the phase transition of MFM-722(Pb)-DMA to form MFM-722(Pb)-H_2O at various times under 98% RH and 25 °C

Time (hours)	Resistance (Ω)	Proton conductivity (S cm^{-1})	MFM-722(Pb)-DMA
0	3.72×10^7	3.64×10^{-5}	↓
1	2.85×10^7	4.76×10^{-5}	
2	2.19×10^7	6.17×10^{-5}	
9	1.67×10^7	8.09×10^{-5}	
13	1.12×10^7	1.21×10^{-4}	
30	1.02×10^7	1.33×10^{-4}	MFM-722(Pb)-H_2O

For the single crystal in Fig. 2b-d ($325 \times 41 \times 31$μm^3), the cross-sectional area (A) is 1.271×10^{-5} cm^2, the length (L) is 3.25×10^{-2} cm; the resistance (R) and proton conductivity (σ) results are summarised in Table S6.

Table S6 Summary of proton conductivity measurements of single crystal MFM-722(Pb)-H_2O at various temperature under 98% RH

temperature (°C)	Resistance (Ω)	Proton conductivity (S cm^{-1})
25	1.57×10^7	1.63×10^{-4}
30	1.18×10^7	2.16×10^{-4}
35	1.06×10^7	2.41×10^{-4}
40	7.27×10^6	3.51×10^{-4}
45	5.30×10^6	4.82×10^{-4}
50	3.87×10^6	6.61×10^{-4}
55	4.29×10^6	5.96×10^{-4}
60	4.63×10^6	5.52×10^{-4}
65	6.11×10^6	4.18×10^{-4}
70	5.91×10^6	4.33×10^{-4}
75	7.20×10^6	3.55×10^{-4}

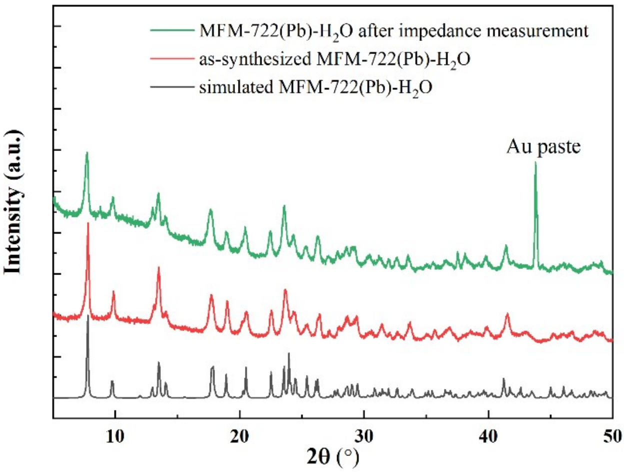

Fig. S19 PXRD patterns of as-synthesized MFM-722(Pb)-H_2O (red), and simulation (black) and after impedance measurement (green).

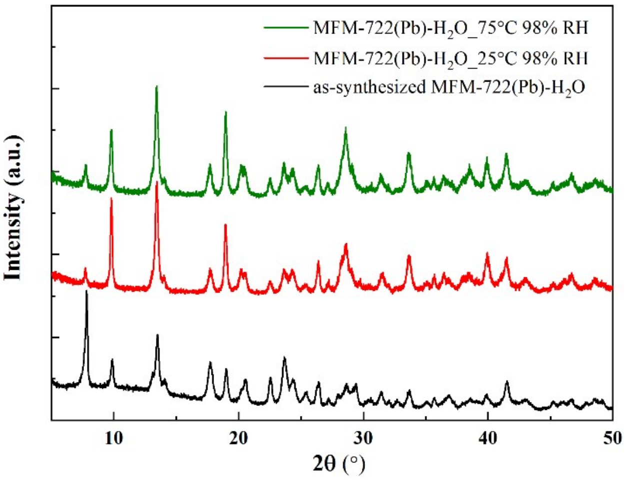

Fig. S20 PXRD patterns of as synthesized MFM-722(Pb)-H_2O (black), MFM-722(Pb)-H_2O at 25 ^oC and 98% RH (red), and of MFM-722(Pb)-H_2O at 75 ^oC and 98% RH (green).

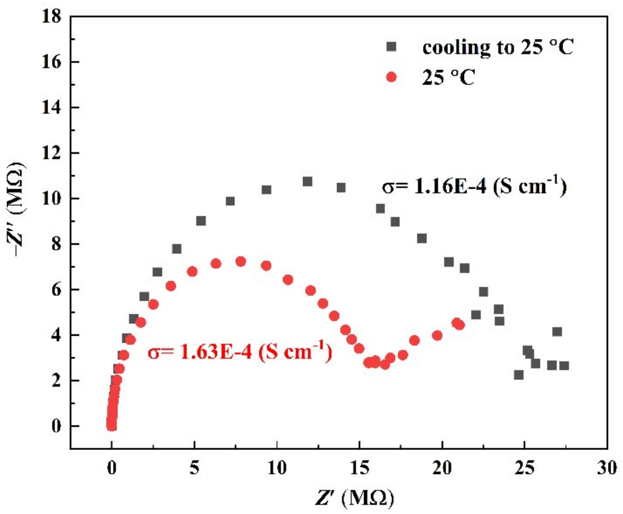

Fig. S21 Nyquist plots for a single crystal of MFM-722(Pb)-H_2O at 25 °C, and at 25 °C after heating to 75 °C at 98% RH.

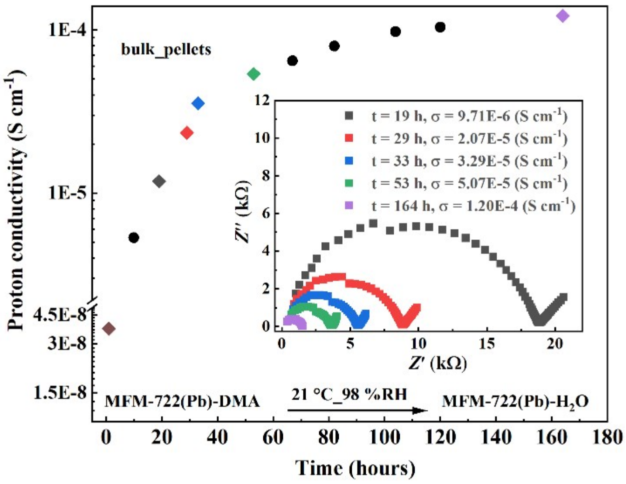

Fig. S22 Time dependence of the bulk pellets proton conductivity during the phase transition from MFM-722(Pb)-DMA to MFM-722(Pb)-H_2O at 21 °C and 98% RH.

Compared with the Nyquist plots of the single crystal of MFM-722(Pb)-H_2O (Fig. 2a), the Nyquist plots of the bulk materials as a pellet also show a typical semi-circle in the high frequency region indicative of the intrinsic conductivity of the material, with the tail at low frequency representing the blocking of protons at the electrode interface. Over prolonged exposure to water vapour, the semi-circle decreases in both cases, indicating the presence of phase transition from MFM-722(Pb)-DMA to MFM-722(Pb)-H_2O.

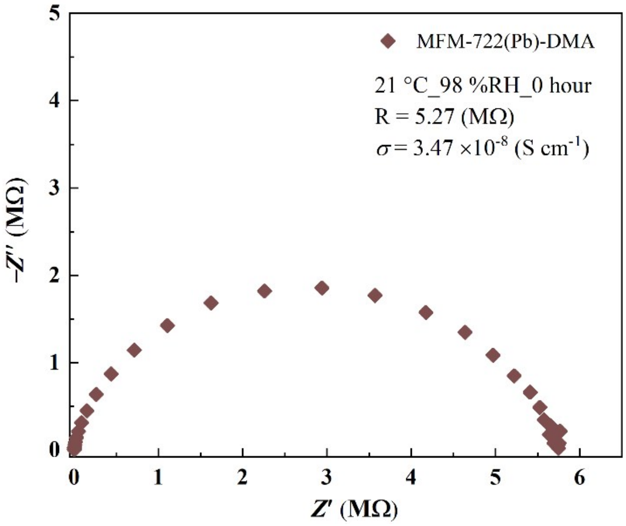

Fig. S23 Nyquist plots of bulk MFM-722(Pb)-DMA at 21 °C and 98% RH at time 0. For this pellet, the cross-sectional area (A) was 0.5027 cm^2 and the length (L) 0.092 cm.

Table S7 Summary of proton conductivity measurements of bulk pellets during the phase transition from MFM-722(Pb)-DMA to MFM-722(Pb)-H_2O at 21 °C and 98%RH.

Time (hours)	Resistance (Ω)	Proton conductivity (S cm^{-1})	
0	5.27×10^{6}	3.47×10^{-8}	MFM-722(Pb)-DMA
10	5.92×10^{4}	3.09×10^{-6}	↓
19	1.88×10^{4}	9.71×10^{-6}	
29	8.84×10^{3}	2.07×10^{-5}	
33	5.57×10^{3}	3.29×10^{-5}	
53	3.61×10^{3}	5.07×10^{-5}	
67	2.99×10^{3}	6.13×10^{-5}	
82	2.39×10^{3}	7.66×10^{-5}	
104	1.93×10^{3}	9.51×10^{-5}	
120	1.81×10^{3}	1.01×10^{-4}	MFM-722(Pb)-H_2O
164	1.52×10^{3}	1.20×10^{-4}	

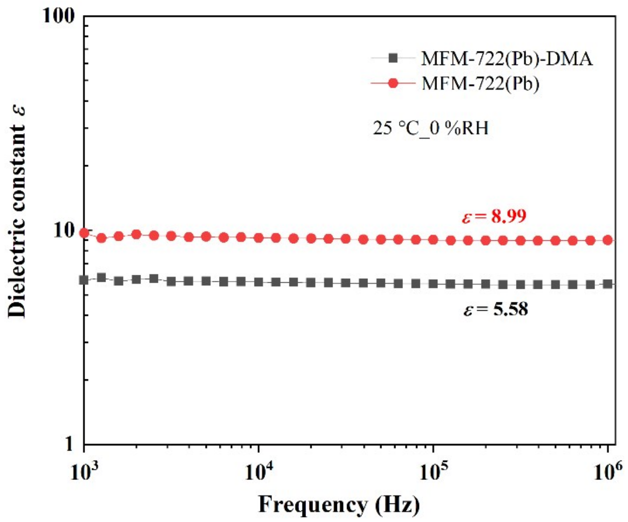

Fig. S24 Dielectric constant measurements for MFM-722(Pb)-DMA and MFM-722(Pb).

Table S8 Comparison of proton conductivity data for related systems from the literature

Compounds	Crystallinity	BET (N_2 77K)	T (°C)	RH (%)		σ (S cm^{-1})	Reference
Pb-BSDC	single crystal	not given	90	85		1.71×10^{-2}	5
	bulk pellet		90	90		1.43×10^{-4}	
$[Pt(dach)(bpy)]_4(SO_4)_4$	single crystal	not given	55	95		1.70×10^{-2}	6
	bulk pellet		65	95		1.66×10^{-3}	
MIP-202(Zr)	bulk pellet	not given	90	95		1.10×10^{-2}	7
MFM-500(Ni)	bulk pellet	< 10 m^2/g	25	98		4.50×10^{-4}	8
MFM-500(Co)			25	98		4.40×10^{-5}	
MFM-550(Ho)	bulk pellet	< 5 m^2/g	20	99		2.51×10^{-4}	9
$Cd_2(TTFTB)$	single crystal	470-537 m^2/mmol	25	35-45 (in the air)		2.86×10^{-4}	10
$Mn_2(TTFTB)$						8.64×10^{-5}	
$Co_2(TTFTB)$						1.49×10^{-5}	
$Zn_2(TTFTB)$						3.95×10^{-6}	
Cd(PYTPY)(TDC)	single crystal	not given	25	35-45 (in the air)		2.85×10^{-9}	11
$Fe_2(DSBDC)(DMF)_2\cdot x(DMF)$	bulk pellet	not given	25	0 (air free)		3.90×10^{-6}	SC-SC transformation 12
$Fe_2(DSBDC)(DMF)_2$		not given				5.80×10^{-7}	
$Fe_2(DSBDC)$		624 m^2/g				1.50×10^{-9}	
$[Ni(H_2L)(bpyBr)_2]\cdot2H_2O$	Membrane in Nafion	not given	60	air		8.89×10^{-7}	SC-SC transformation 13
$[Ni_2(H_2L)_2(bpyBr)_2(H_2O)_3]_n$			60	air		7.43×10^{-7}	
$[Cu(HL)\text{-}(DMSO)]_n$	bulk pellet	< 1 m^2/g	25	55		5.88×10^{-8}	SC-SC transformation 14
$H_3L\cdot0.5[Cu_2(OH)_4\cdot6H_2O]\cdot4H_2O$			25	95		7.42×10^{-4}	
			60	95		5.48×10^{-3}	
MFM-722(Pb)-DMA	single crystal	83 m^2/g	25	98	0 hour	3.64×10^{-5}	SC-SC transformation This work
	bulk pellet		21	98	0 hour	3.47×10^{-8}	
$MFM\text{-}722(Pb)\text{-}H_2O$	single crystal	32 m^2/g	25	98	> 10 hours	1.33×10^{-4}	
	single crystal		50	98		6.61×10^{-4}	
	bulk pellet		21	98	> 100 hours	1.20×10^{-4}	

Abbreviations in Table S8: H_4BSDC^{4-} = 2,2'-disulfomethyl-[1,1'-biphenyl]-4,4'-dicarboxylate; dach = (1R, 2R)-(–)-1,2-diaminocyclohexane; bpy = 1,4-bipyridine; $DSBDC^{4-}$ = 2,5-disulfidobenzene-1,4-dicarboxylate; $TTFTB^{4-}$ = tetrathiafulvalene tetrabenzoate; PYTPY = 4′-(4-pyridyl)2,2′:6′,2″-terpyridine; MIP-202(Zr) = $[Zr_6O_4(OH)_4(Aspartate)_6(HCl)_6]\cdot nH_2O$; MFM-550(M) = $[M(C_{12}H_8P_2O_6H)]$; TDC^{2-} = 2,5-thiophenedicarboxylate.

Table S9. Comparison of crystallographic data of MFM-722(Pb)-H_2O at 100 K and 298 K.

Name	MFM-722(Pb)-H_2O	
Temperature, K	100 K	298 K
Formula	$C_{16}H_8O_9Pb_2$ $[Pb_2(L)(H_2O)]$	$C_{16}H_8O_9Pb_2$ $[Pb_2(L)(H_2O)]$
Radiation	CuKα (λ = 1.5418)	CuKα (λ = 1.5418)
Crystal system	Triclinic	Triclinic
Space group	$P\bar{1}$	$P\bar{1}$
a, Å	7.3121(17)	7.3354(15)
b, Å	9.4816(17)	9.5103(16)
c, Å	11.803(3)	11.9815(19)
α, deg	81.482(17)	80.532(14)
β, deg	74.95(2)	74.321(16)
γ, deg	73.334(18)	72.843(16)
V, Å^3	754.6(3)	765.667
Z	2	2

REFERENCES

1. X. Lin, I. Telepeni, A.J. Blake, A. Dailly, C.M. Brown, J. M. Simmons, M. Zoppi, G. S. Walker, K.M. Thomas, T.J. Mays, P. Hubberstey, N.R. Champness and M. Schröder, *J. Am. Chem. Soc.*, 2009, **131**, 2159-2171.
2. CrysAlis, C.C.D. CrysAlis Red, Xcalibur PX Software, Oxford Diffraction Ltd., Abingdon, England, 2008.
3. O. V. Dolomanov, L. J. Bourhis, R. J. Gildea, J. A. K. Howard and H. Puschmann, *J. Appl. Crystall.*, 2009, **42**, 339–341.

4 L. Sun, S. S. Park, D. Sheberla and M. Dincă, *J. Am. Chem. Soc.*, 2016, **138**, 14772–14782.

5 H. Zhang, Z.-A. Yan, Z.-M. Wu, Z.-Q. Lin, W.-M. Liao and J. He, *J. Solid State Chem.*, 2020, **287**, 121325.

6 K. Otake, K. Otsubo, T. Komatsu, S. Dekura, J. M. Taylor, R. Ikeda, K. Sugimoto, A. Fujiwara, C.-P. Chou, A. W. Sakti, Y. Nishimura, H. Nakai and H. Kitagawa, *Nat. Comm.,* 2020, 11, 843.

7 S. Wang, M. Wahiduzzaman, L. Davis, A. Tissot, W. Shepard, J. Marrot, C. Martineau-Corcos, D. Hamdane, G. Maurin, S. Devautour-Vinot and C. Serre, *Nat. Comm.*, 2018, **9**, 4937.

8 S. Pili, S. P. Argent, C. G. Morris, P. Rought, V. García-Sakai, I. P. Silverwood, T. L. Easun, M. Li, M. R. Warren, C. A. Murray, C. C. Tang, S. Yang and M. Schröder, *J. Am. Chem. Soc.*, 2016, **138**, 6352–6355.

9 S. Pili, P. Rought, D. I. Kolokolov, L. Lin, I. da Silva, Y. Cheng, C. Marsh, I. P. Silverwood, V. García Sakai, M. Li, J. J. Titman, L. Knight, L. L. Daemen, A. J. Ramirez-Cuesta, C. C. Tang, A. G. Stepanov, S. Yang and M. Schröder, *Chem. Mat.*, 2018, **30**, 7593–7602.

10 S. S. Park, E. R. Hontz, L. Sun, C. H. Hendon, A. Walsh, T. Van Voorhis and M. Dincă, *J. Am. Chem. Soc.*, 2015, **137**, 1774–1777.

11 J. Huang, J. Zhang, R. He and Z. Fu, *CrystEngComm*, 2018, **20**, 5663–5666.

12 L. Sun, C. H. Hendon and M. Dincă, *Dalton Trans.*, 2018, **47**, 11739–11743.

13 R.-Y. Li, H.-T. Liu, C.-C. Zhou, Z.-T. Chu, J. Lu, S.-N. Wang, J. Jin and W.-F. Yan, *Inorg. Chem. Front.*, 2020, **7**, 1880-1891.

14 S. Nakatsuka, Y. Watanabe, Y. Kamakura, S. Horike, D. Tanaka and T. Hatakeyama, *Angew. Chem. Int. Ed.*, 2020, **59**, 1435–1439.